Elena Lazzeri · Alberto Signore
Paola Anna Erba · Napoleone Prandini
Annibale Versari · Giovanni D´Errico
Giuliano Mariani *Editors*

Radionuclide Imaging of Infection and Inflammation

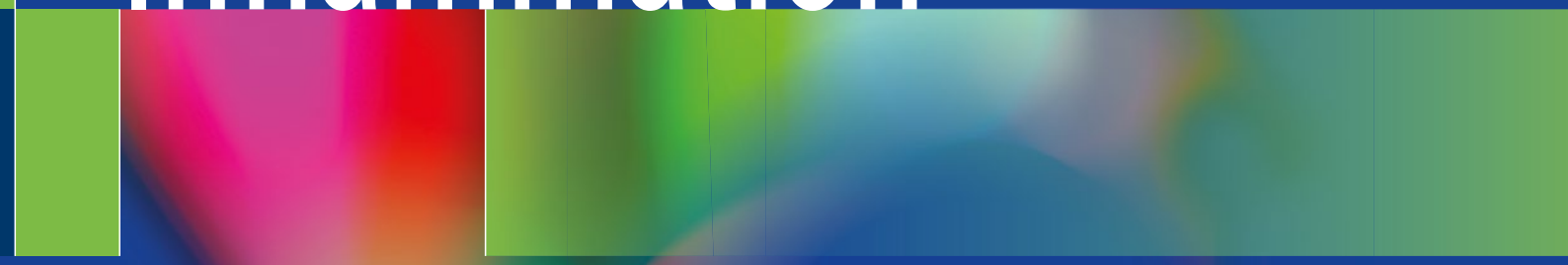

A Pictorial Case-Based Atlas

Second Edition

Springer

Radionuclide Imaging of Infection and Inflammation

Elena Lazzeri • Alberto Signore
Paola Anna Erba • Napoleone Prandini
Annibale Versari • Giovanni D´Errico
Giuliano Mariani
Editors

Radionuclide Imaging of Infection and Inflammation

A Pictorial Case-Based Atlas

Second Edition

Springer

Editors
Elena Lazzeri
Regional Center of Nuclear Medicine
University Hospital of Pisa
Pisa
Italy

Paola Anna Erba
Department of Translational Research and
Advanced Technologies in Medicine and Surgery,
Regional Center of Nuclear Medicine
University of Pisa
Pisa
Italy

Annibale Versari
Nuclear Medicine
Azienda Unità Sanitaria Locale-IRCCS di Reggio
Emilia
Reggio Emilia
Italy

Giuliano Mariani
Department of Translational Research and
Advanced Technologies in Medicine and Surgery,
Regional Center of Nuclear Medicine
University of Pisa
Pisa
Italy

Alberto Signore
Department of Medical-Surgical Sciences
and of Translational Medicine
Sapienza University of Rome
Roma
Italy

Napoleone Prandini
Nuclear Medicine Department
Azienda Ospedaliero-Universitaria di Modena
Modena
Italy

Giovanni D´Errico
Nuclear Medicine Department
Private Hospital "PIO XI"
Roma
Italy

ISBN 978-3-030-62174-2 ISBN 978-3-030-62175-9 (eBook)
https://doi.org/10.1007/978-3-030-62175-9

This Springer imprint is published by the registered company Springer Nature Switzerland AG
The registered company address is: Gewerbestrasse 11, 6330 Cham, Switzerland

Foreword

Molecular imaging with positron emission tomography (PET) and single-photon computed tomography (SPECT) combined with computed tomography (CT) is increasingly being used in Nuclear Medicine to diagnose, characterize, and monitor disease activity in the setting of infections and inflammatory disorders. Hybrid PET/CT and SPECT/CT both produce images based on the biodistribution of radiopharmaceuticals able to localize the inflammatory changes and to describe their response to therapy. Although several textbooks have been published on this subject, the most successful so far has been *Radionuclide Imaging of Infection and Inflammation: A Pictorial Case-Based Atlas* (published by Springer in 2013) that presented and discussed a whole host of clinical cases and imaging examples illustrating the manifestations of the commonly encountered infectious and inflammatory conditions.

This new textbook is the second edition of the same Atlas, still edited by *Elena Lazzeri, Alberto Signore, Paola Anna Erba, Napoleone Prandini, Annibale Versari, Giovanni D'Errico, and Giuliano Mariani*. Until now the first edition has been considered an important and successful reference for medical students, residents in nuclear medicine and radiology, and for all physicians involved in the management of patients with infection and inflammation. The main added value of the Atlas was both the high level of its scientific contents and the original structure of its educational contents. Alongside the description of the most important inflammatory and infectious diseases, the authors presented in each chapter a series of illustrated teaching cases with images of the most frequent scintigraphic findings, as well the anatomic variants and technical pitfalls. Thus, the reader had the opportunity to understand the pathophysiologic basis of infections and inflammation and to learn how to correctly interpret the images obtained with these studies.

Several years have now elapsed since that first very lucky edition, which received the general appreciation of the clinical and scientific community. Over this period scientific knowledge of the molecular mechanisms and biology of the inflammatory response has changed. The same happened for infections, which today show different patterns versus those most frequently observed previously; in particular, the spectrum of pathogen agents, including viruses, has changed over time and new infections have emerged. New guidelines and recommendations have been developed by scientific societies, some of them with direct or indirect effects on the indications for some nuclear medicine imaging procedures. Furthermore, important technological advances have taken place in nuclear medicine concerning both imaging instrumentation and radiopharmaceuticals.

The above reasons stimulated the authors to implement, integrate, and enlarge the first edition of the Atlas to become this textbook. This second edition maintains the same excellent original structure based on accurate information on the diseases, technologies, and case reports with a high number of associated images, addressing the common questions and problems that arise in the daily practice. Furthermore, the number of chapters has been increased from 13 to 16, the new chapters being devoted to miscellaneous bone and joint conditions, to inflammatory vessels' disease (vasculitis and atherosclerosis), and to infections and inflammation in pediatrics. All the chapters have been modified and/or rewritten to address the latest advancements in the field. References have been carefully updated and new clinical cases have been included and discussed according to the most recent protocols and guidelines.

This new edition of the Atlas is still organized by clinical entity, and all issues are clearly presented, well illustrated, and referenced. Clinical cases at the end of each chapter offer a good teaching tool that refreshes and supports the concepts discussed in the main text. The illustrations are of very high quality, most of them being illustrated with hybrid imaging. The contents of the textbook cover all indications of nuclear medicine imaging in the current scenario of infections and inflammation. The book begins with the normal findings by using different radiopharmaceuticals and techniques, discussing variants and pitfalls. The following three chapters are devoted to imaging of soft tissue infections, bone and joint infections, and imaging of miscellaneous bone and joint conditions. Joint prosthesis infections and peripheral bone infections, vascular prosthesis infections, and nonorthopedic or cardiovascular implantable device infections are discussed in the following chapters. Other chapters are dedicated to some less known or less frequent conditions, such as inflammation of the head and neck region (including the central nervous system), infective endocarditis and cardiovascular implantable electronic devices, and fever of unknown origin. The textbook also presents abdominal infections and inflammations, diabetic foot infections, lung infections, chronic inflammatory diseases, inflammatory vascular diseases, vasculitis and atherosclerosis, and finally infections and inflammation in pediatrics.

In conclusion, this renewed Atlas continues to offer an excellent example of a modern and educational textbook, which is intended to disseminate worldwide the most up-to-date knowledge on the current role of nuclear medicine in the field. The authors, among the most experienced and distinguished professionals in this field, accomplished a great work to keep the contents of this text at the highest level, and through a multidisciplinary approach they have implemented an exceptional learning tool very useful for all physicians with interest in radionuclide imaging of infection and inflammation.

Bergamo, Italy
May 2020

Emilio Bombardieri

Preface

Why a second edition of *Radionuclide Imaging of Infection and Inflammation: A Pictorial Case-Based Atlas*? This is the question that most people looking at this textbook will wonder about. The answer is easy: being an atlas of images and interesting cases, there are always more cases and more educational images to add, in order to improve the understanding of the role of nuclear medicine imaging in the field of infection and inflammation. Furthermore, in the time elapsed since the first edition the role of [^{18}F]FDG PET/CT for imaging infection and/or inflammation has greatly expanded. At the same time, hybrid imaging with SPECT/CT has revived interest in single-photon imaging for infection, and new radiotracers are being developed for imaging of infection/inflammation.

It comes as a second consideration that this new edition is not intended to merely replace the first one, but rather to integrate it—so that the two editions will constitute a unicum, a full educational tool for all physicians with interest in radionuclide imaging of infection and inflammation.

As in the first edition of the book, we kept the same chapters, but raised the number from 13 to 16 in order to address the growing applications of radionuclide imaging for infection and inflammation, with particular emphasis on inflammatory vessels' conditions, such as vasculitis and atherosclerosis and on infection and inflammation in pediatrics.

Furthermore, the structure of each chapter has been modified to include learning objectives for each chapter and key learning points for each condition. This is an important modification that provides to the reader the possibility to quickly focus on the most relevant aspects for correct interpretation of images.

Finally, the most relevant feature of this second edition is that text and images have been prepared according to the multidisciplinary guidelines developed by the European Association of Nuclear Medicine (EANM) in conjunction with several other European societies of clinicians and radiologists; a list of the most relevant of such joint guidelines is reported in the next page. Therefore, this textbook is not the mere result of the experience of a group of Italian nuclear medicine physicians, but rather the summary of a wide international experience in the field. Indeed, some of the authors have been involved for several years in international task groups or committees of several world leading scientific societies.

This upgrade makes the book a modern and up-to-date reference manual for students and physicians who are approaching or already working in this field of nuclear medicine.

Rome, Italy — Alberto Signore
Rome, Italy — Giovanni D'Errico
Pisa, Italy — Paola Anna Erba
Pisa, Italy — Elena Lazzeri
Modena, Italy — Napoleone Prandini
Reggio Emilia, Italy — Annibale Versari
Pisa, Italy — Giuliano Mariani

April 2020

List of International Guidelines on Radionuclide Imaging of Infection/ Inflammation Imaging (Most Recent Publications Listed First)

Dorbala S, Ando Y, Bokhari S, Dispenzieri A, Falk RH, Ferrari VA, et al. ASNC/AHA/ASE/EANM/HFSA/ISA/SCMR/SNMMI expert consensus recommendations for multimodality imaging in cardiac amyloidosis: part 2 of 2—diagnostic criteria and appropriate utilization. J Nucl Cardiol. 2020;27:659–73.

Dorbala S, Ando Y, Bokhari S, Dispenzieri A, Falk RH, Ferrari VA, et al. ASNC/AHA/ASE/EANM/HFSA/ISA/SCMR/SNMMI expert consensus recommendations for multimodality imaging in cardiac amyloidosis: part 1 of 2—evidence base and standardized methods of imaging. J Nucl Cardiol. 2019;26:2065–123.

Lazzeri E, Bozzao A, Cataldo MA, Petrosillo N, Manfrè L, Trampuz A, et al. Joint EANM/ESNR and ESCMID-endorsed consensus document for the diagnosis of spine infection (spondylodiscitis) in adults. Eur J Nucl Med Mol Imaging. 2019;46:2464–87.

Sconfienza LM, Signore A, Cassar-Pullicino V, Cataldo MA, Gheysens O, Borens O, et al. Diagnosis of peripheral bone and prosthetic joint infections: overview on the consensus documents by the EANM, EBJIS, and ESR (with ESCMID endorsement). Eur Radiol. 2019;29:6425-6438.

Signore A, Sconfienza LM, Borens O, Glaudemans AWJM, Cassar-Pullicino V, Trampuz A, et al. Consensus document for the diagnosis of prosthetic joint infections: a joint paper by the EANM, EBJIS, and ESR (with ESCMID endorsement). Eur J Nucl Med Mol Imaging. 2019;46:971–88.

Glaudemans AWJM, Jutte PC, Cataldo MA, Cassar-Pullicino V, Gheysens O, Borens O, et al. Consensus document for the diagnosis of peripheral bone infection in adults: a joint paper by the EANM, EBJIS, and ESR (with ESCMID endorsement). Eur J Nucl Med Mol Imaging. 2019;46:957–70.

Slart RHJA; Writing group; Reviewer group; Members of EANM Cardiovascular; Members of EANM Infection & Inflammation; Members of Committees, SNMMI Cardiovascular; Members of Council, PET Interest Group; Members of ASNC; EANM Committee Coordinator. FDG-PET/CT(A) imaging in large vessel vasculitis and polymyalgia rheumatica: joint procedural recommendation of the EANM, SNMMI, and the PET Interest Group (PIG), and endorsed by the ASNC. Eur J Nucl Med Mol Imaging. 2018;45:1250–69.

Signore A, Jamar F, Israel O, Buscombe J, Martin-Comin J, Lazzeri E. Clinical indications, image acquisition and data interpretation for white blood cells and anti-granulocyte monoclonal antibody scintigraphy: an EANM procedural guideline. Eur J Nucl Med Mol Imaging. 2018;45:1816–31.

Van den Wyngaert T, Strobel K, Kampen WU, Kuwert T, van der Bruggen W, Mohan HK, et al. The EANM practice guidelines for bone scintigraphy. Eur J Nucl Med Mol Imaging. 2016;43:1723–38.

Bucerius J, Hyafil F, Verberne HJ, Slart RH, Lindner O, Sciagrà R, et al. Position paper of the Cardiovascular Committee of the European Association of Nuclear Medicine (EANM) on PET imaging of atherosclerosis. Eur J Nucl Med Mol Imaging. 2016;43:780–92.

Habib G, Lancellotti P, Antunes MJ, Bongiorni MG, Casalta JP, Del Zotti F, et al. 2015 ESC guidelines for the management of infective endocarditis: the Task Force for the Management of Infective Endocarditis of the European Society of Cardiology (ESC). Endorsed by: European

Association for Cardio-Thoracic Surgery (EACTS), the European Association of Nuclear Medicine (EANM). Eur Heart J. 2015;36:3075–128.

Jamar F, Buscombe J, Chiti A, Christian PE, Delbeke D, Donohoe KJ, et al. EANM/SNMMI guideline for ^{18}F-FDG use in inflammation and infection. J Nucl Med. 2013;54:647–58.

Panes J, Bouhnik Y, Reinisch W, Stoker J, Taylor SA, Baumgart DC, et al. Imaging techniques for assessment of inflammatory bowel disease: joint ECCO and ESGAR evidence-based consensus guidelines. J Crohns Colitis. 2013;7:556–85.

de Vries EF, Roca M, Jamar F, Israel O, Signore A. Guidelines for the labelling of leucocytes with ^{99m}Tc-HMPAO. Inflammation/Infection Taskgroup of the European Association of Nuclear Medicine. Eur J Nucl Med Mol Imaging. 2010;37:842–8.

Roca M, de Vries EF, Jamar F, Israel O, Signore A. Guidelines for the labelling of leucocytes with ^{111}In-oxine. Inflammation/Infection Taskgroup of the European Association of Nuclear Medicine. Eur J Nucl Med Mol Imaging. 2010;37:835–41.

Contents

Contributors

Francesco Bandera Department of Biomedical Sciences for Health, University of Milan, Milan, Italy

Cardiology University Department, Heart Failure Unit, IRCCS Policlinico San Donato, San Donato Milanese, Milan, Italy

Francesco Bartoli Department of Translational Research and Advanced Technologies in Medicine and Surgery, Regional Center of Nuclear Medicine, University of Pisa, Pisa, Italy

Andrea Bedini Infectious Diseases Unit, Department of Medical and Surgical Sciences for Children and Adults, University Hospital "Policlinico di Modena", Modena, Italy

Florent L. Besson Department of Biophysics and Nuclear Medicine-Molecular Imaging, Hôpitaux Universitaires Paris-Saclay, Assistance Publique-Hôpitaux de Paris, CHU Bicêtre, Le Kremlin Bicêtre, France

Université Paris Saclay, CEA, CNRS, Inserm, BioMaps, Orsay, France

Jan Bucerius Department of Nuclear Medicine, University Medicine Göttingen, Georg-August-University Göttingen, Göttingen, Germany

Massimiliano Casali Nuclear Medicine, Azienda Unità Sanitaria Locale-IRCCS of Reggio Emilia, Reggio Emilia, Italy

Emanuele Casciani Department of Nuclear Medicine, Private Hospital "Pio XI", Rome, Italy

Giovanni D'Errico Department of Nuclear Medicine, Private Hospital "Pio XI", Rome, Italy

Paola Anna Erba Department of Translational Research and Advanced Technologies in Medicine and Surgery, Regional Center of Nuclear Medicine, University of Pisa, Pisa, Italy

Maria Carmen Garganese Nuclear Medicine Unit, Department of Imaging, "Bambino Gesù" Pediatric Hospital, Rome, Italy

Tiziana Lanzolla Nuclear Medicine Unit, AOU Sant'Andrea, Rome, Italy

Chiara Lauri Department of Medical-Surgical Sciences and of Translational Medicine, Sapienza University of Rome, Rome, Italy

Nuclear Medicine Unit, AOU Sant'Andrea, Rome, Italy

Elena Lazzeri Regional Center of Nuclear Medicine, University Hospital of Pisa, Pisa, Italy

Giuliano Mariani Department of Translational Research and Advanced Technologies in Medicine and Surgery, Regional Center of Nuclear Medicine, University of Pisa, Pisa, Italy

Napoleone Prandini Nuclear Medicine Department, Azienda Ospedaliero-Universitaria di Modena, Modena, Italy

Alberto Signore Department of Medical-Surgical Sciences and of Translational Medicine, Sapienza University of Rome, Roma, Italy

Nuclear Medicine Unit, AOU Sant'Andrea, Rome, Italy

Riemer H. J. A. Slart Medical Imaging Center, Department of Nuclear Medicine and Molecular Imaging, University of Groningen, University Medical Center Groningen, Groningen, The Netherlands

Department of Biomedical Photonic Imaging, Faculty of Science and Technology, University of Twente, Enschede, The Netherlands

Saadi Sollaku Department of Nuclear Medicine, Private Hospital "Pio XI", Rome, Italy

Martina Sollini Department of Biomedical Sciences, Humanitas University, Pieve Emanuele, Italy

Humanitas Clinical and Research Center - IRCCS, Rozzano, Italy

Annibale Versari Nuclear Medicine, Azienda Unità Sanitaria Locale-IRCCS di Reggio Emilia, Reggio Emilia, Italy

Maria Felicia Villani Nuclear Medicine Unit, Department of Imaging, "Bambino Gesù" Pediatric Hospital, Rome, Italy

Roberta Zanca Department of Translational Research and Advanced Technologies in Medicine and Surgery, Regional Center of Nuclear Medicine, University of Pisa, Pisa, Italy

Normal Findings with Different Radiopharmaceuticals, Techniques, Variants, and Pitfalls

1

Annibale Versari and Massimiliano Casali

Contents

A. Versari (✉) ·
Nuclear Medicine, Azienda Unità Sanitaria Locale-IRCCS di Reggio Emilia, Reggio Emilia, Italy
e-mail: annibale.versari@ausl.re.it

M. Casali
Nuclear Medicine, Azienda Unità Sanitaria Locale-IRCCS of Reggio Emilia, Reggio Emilia, Italy

E. Lazzeri et al. (eds.), *Radionuclide Imaging of Infection and Inflammation*, https://doi.org/10.1007/978-3-030-62175-9_1

Learning Objectives

- To acquire basic knowledge on the main nuclear medicine techniques applied to the diagnosis and monitoring of inflammatory and infectious processes
- To focus the attention on biodistribution, normal variants and the main diagnostic pitfalls of the "old" and the "newest" nuclear medicine agents, the latter including radiolabeled UBI-fragments, [^{18}F]FDG-labeled leukocytes, ^{68}Ga-citrate, and ^{124}I-Fiualuridine for PET imaging
- To shed light on the possibile use of radiolabeled antibiotics for the scintigraphic detection of infections

1.1 Introduction

The pharmacokinetic and/or pharmacodynamic patterns of radiopharmaceuticals in patients may be affected by several factors including a variety of drugs, disease states, and, in some cases, surgical procedure [1]. Among the factors that can change radiopharmaceutical biodistribution, co-administration of interfering drugs is the most commonly reported occurrence [2]. Drug–radiopharmaceutical interactions may arise as a result of the mode of drug action, of physico-chemical interactions between drugs and radiotracers, and of competition for common binding sites [2–4].

Table 1.1 lists drugs that can interfere with the biodistribution of ^{67}Ga-citrate, radiolabeled autologous leukocytes, and [^{18}F]FDG in patients [5].

Also faulty radiopharmaceutical preparation (including contamination during dispensing or administration and errors in the labeling procedure of autologous leukocytes with ^{111}In-oxine or ^{99m}Tc-HMPAO) may alter the subsequent biodistribution of radiopharmaceuticals, thus affecting the diagnostic quality of scintigraphic images [3, 6–12]. Although less commonly, radiopharmaceuticals may also interact with the syringe's or intravenous line's components [13, 14]. Also some lifestyle factors such as smoking, alcohol intake, and dietary habits (i.e., high-dose vitamins) have the potential of interacting with radiopharmaceuticals [15]. Furthermore, the use of monoclonal antibodies of murine origin may induce generation of human antimouse antibodies (HAMA), which can lead to allergic reactions and altered pharmacokinetics upon repeated injections [16].

Finally, technical pitfalls that may affect the results of imaging include equipment-related artifacts (i.e., inadequate quality-control procedures/calibration) as well as image processing-related artifacts (i.e., misregistration of the CT component with the SPECT or PET component), patient-related artifacts (i.e., patient motion) [6], and radiopharmaceutical extravasation during administration [6, 17, 18] (Fig. 1.1).

Tables 1.2 and 1.3 summarize the main pathophysiological characteristics and biodistribution of the radiopharmaceutical preparations discussed in this chapter [16].

Table 1.1 Drugs that can interfere with biodistribution of the radiopharmaceuticals/procedures most commonly employed for imaging inflammatory and infectious diseases (adapted from AIMN procedural Guide-Lines: http://www.aimn.it/pubblicazioni/LG/RP_AIMN_infezioni.pdf)

Radiopharmaceutical	Pharmaceutical class	Drug
^{67}Ga-citrate ^{68}Ga-citrate	Mineral supplements	Iron Calcium gluconate (parenteral)
	Chemotherapeutics	All
	Steroids	Prednisolone
Radiolabeled leukocytes	Beta lactam antibiotics	Cefalosporin
	Immunosuppressive	Azathioprine Cyclophosphamide
	Steroids	Prednisolone
	Calcium-antagonists	Nifedipine
	Anticoagulants	Heparin
	Sulfamide	Sulfasalazine
	Iron	Iron
[^{18}F]FDG	Steroids	Prednisolone
	Antiepileptics	Valproate Carbamazepine Phenytoin Phenobarbital
	Catecholamines	Catecholamines

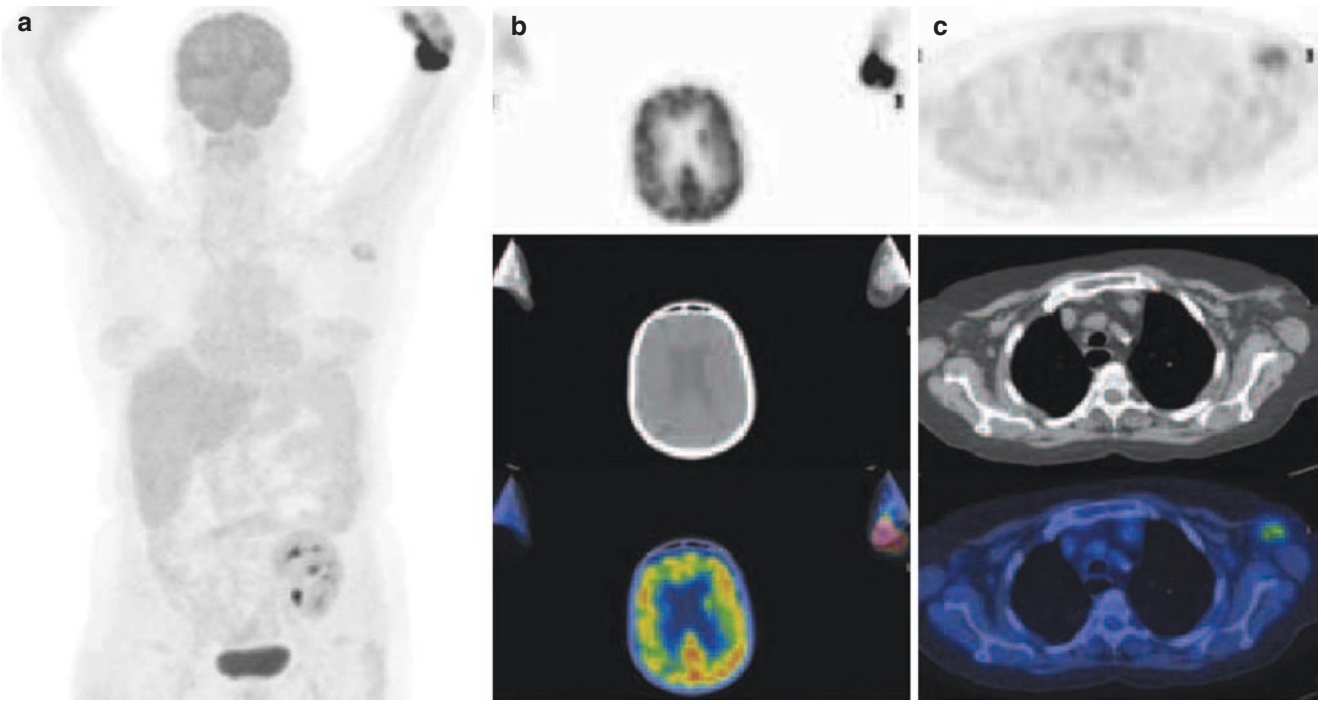

Fig. 1.1 MIP [^{18}F]FDG PET/CT image (**a**) shows intense radiopharmaceutical localization at injection site (left arm) as confirmed by transaxial views (**b**) associated with mild uptake in the left axilla (**c**) due to lymphatic drainage after [^{18}F]FDG extravasation during administration

Table 1.2 Targeting mechanisms of the radiopharmaceutical preparations most commonly employed for imaging inflammatory/infectious disease (modified from Laverman P et al. Current Radiopharmaceuticals. 2008)

Physiological characteristics	Targeting mechanism	Radiopharmaceutical
Enhanced vascular permeability	Transferrin and lactoferrin receptor binding	^{67}Ga-citrate ^{68}Ga-citrate
Enhanced vascular permeability and increased bone metabolism	Adsorption on hydroxyapatite crystals	^{99m}Tc-methylene diphosphonate (MDP)
Enhanced vascular permeability and endothelial activation	Uptake in activated endothelial cells	^{99m}Tc-sulfur colloid ^{99m}Tc-albumin nanocolloids
Enhanced vascular permeability and chemotactic activation	Chemotactic activation	Radiolabeled leukocytes (^{99m}Tc/[^{18}F]FDG)
Enhanced vascular permeability and cell binding	Antigen binding	^{99m}Tc-anti-NCA-95 IgG, BW 250/183, besilesomab (Scintimun®) ^{99m}Tc-anti-SSEA-1 IgM, falonesomab (Leu-Tech®, NutroSpec®) ^{99m}Tc-anti-NCA-90 Fab', Sulesomab (LeukoScan®)
Increased metabolic requirements	Enhanced glucose uptake in activated cells	[^{18}F]FDG
Incorporation into bacteria	Substrate of bacterial thymidine kinase	^{124}I-fialuridine
Electrostatic attraction to bacteria surface	Antimicrobial peptide (AMP) fragment	^{99m}Tc-ubiquicidin

Table 1.3 Physiologic whole-body distribution of the radiopharmaceutical preparations most commonly used for imaging inflammatory/infectious disease (modified from Becker W. The contribution of nuclear medicine to the patient with infection. Eur J Nucl Med. 1995)

Radiopharmaceutical	Liver	Spleen	Kidney	Bladder	Bowel	Bone cortical	Bone marrow	Blood
^{67}Ga/^{68}Ga-citrate	Yes	Yes	Yes	Yes	Yes	No	Yes	No
^{99m}Tc-MDP/HDP	No	No	Yes	Yes	No	Yes	No	No
^{99m}Tc-sulfur colloid and ^{99m}Tc-albumin nanocolloid	Yes	Yes	Yes	Yes	No	No	Yes	No
^{111}In-oxine-leukocytes	Yes	Yes	No	No	No	No	Yes	No
^{99m}Tc-HMPAO-leukocytes	Yes	Yes	Yes	Yes	Yes	No	Yes	No
^{99m}Tc-anti-granulocyte monoclonal antibodies	Yes	Yes	Yes	Yes	No	No	Yes	No
[^{18}F]FDG	Yes	Yes	Yes	Yes	No	No	No	No
Radiolabeled-UBI fragments	No	No	Yes	Yes	No	No	No	No
^{124}I-fialuridine	Yes	Yes	Yes	Yes	No	No	No	No

1.2 ^{67}Ga-Citrate Scintigraphy

1.2.1 Normal Biodistribution of ^{67}Ga-Citrate

About 10–25% of the injected activity is excreted through the kidneys during the first 24 h after administration, after which the principal route of excretion is the large bowel. By 48 h post injection, about 75% of the injected activity remaining in the body is equally distributed among the liver, bone/bone marrow, and soft tissues. ^{67}Ga-citrate localizes in bone marrow because it is incorporated as an iron analog into forming red blood cells; some (low degree) localization in bone is due to the $^{67}Ga^{++}$ ion weakly mimicking distribution of the calcium ions. Localization in the nasopharynx, lacrimal glands, salivary, thymus, breasts, spleen, and genitalia occurs with variable degrees [19–21]. Typical whole-body and spot images acquired at 24 h and 72 h post-injection of ^{67}Ga-citrate are shown in Figs. 1.2 and 1.3, respectively.

1.2.2 Normal Variants in ^{67}Ga-Citrate Scintigraphy

1. Below 2 years of age, increased thymic activity is common [22].
2. Hilar lymph node localization (usually low grade) can be seen in adult patients, particularly in smokers [23].
3. Increased breast activity, which is otherwise generally faint and symmetric, although it can be more intense in patients with hyperprolactinemia (associated physiologically with pregnancy and lactation, but possibly caused by numerous drugs, renal failure, in addition to prolactin-

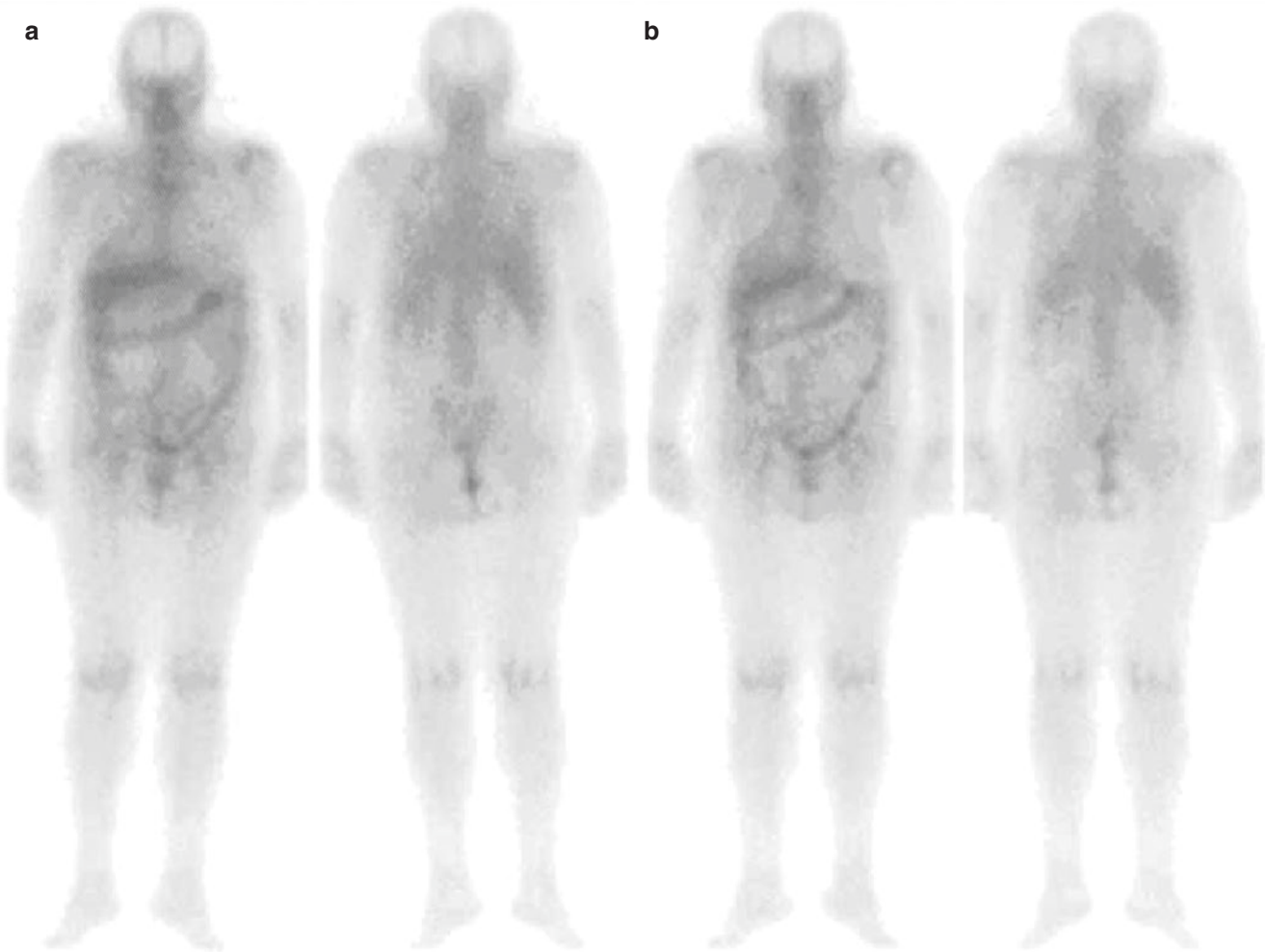

Fig. 1.2 ^{67}Ga-citrate scintigraphy: whole body images in anterior and posterior views obtained 48 h (**a**) and 72 h (**b**) after i.v. administration, showing physiologic biodistribution in the liver, bone and bone marrow, and soft tissues 48 h after injection. Similar pattern of distribution at 72 h. Both the images show radiopharmaceutical localization in the large bowel (major route of excretion from 24 h post-injection onward)

producing pituitary adenomas or to hypothalamic lesions which determine interruption of the hypothalamic–pituitary axis) [24, 25].

1.2.3 Pitfalls in ^{67}Ga-Citrate Scintigraphy

1. Residual bowel activity is probably the most common cause for both false-positive and false-negative interpretations [26], especially if planar images only are acquired rather than SPECT or preferably SPECT/CT images.
2. In children and teenagers, increased activity can be seen in case of thymic hyperplasia secondary to chemotherapy [27].
3. Gadolinium administered for MRI enhancement within 24 h before ^{67}Ga-citrate injection has been reported to decrease localization of the radiopharmaceutical at the sites of interest [28].
4. Saturation of iron-binding transferrin sites (i.e., hemolysis or multiple blood transfusions) causes altered ^{67}Ga distribution, thus resulting in increased renal, bladder, and bone activity and in reduced liver uptake and reduced accumulation in the colon [19].
5. ^{67}Ga uptake at sites of bone repair secondary to healing fractures (or prior orthopedic hardware sites, loose prostheses, or after successful treatment of osteomyelitis) may complicate interpretation in patients with suspected osteomyelitis [29].

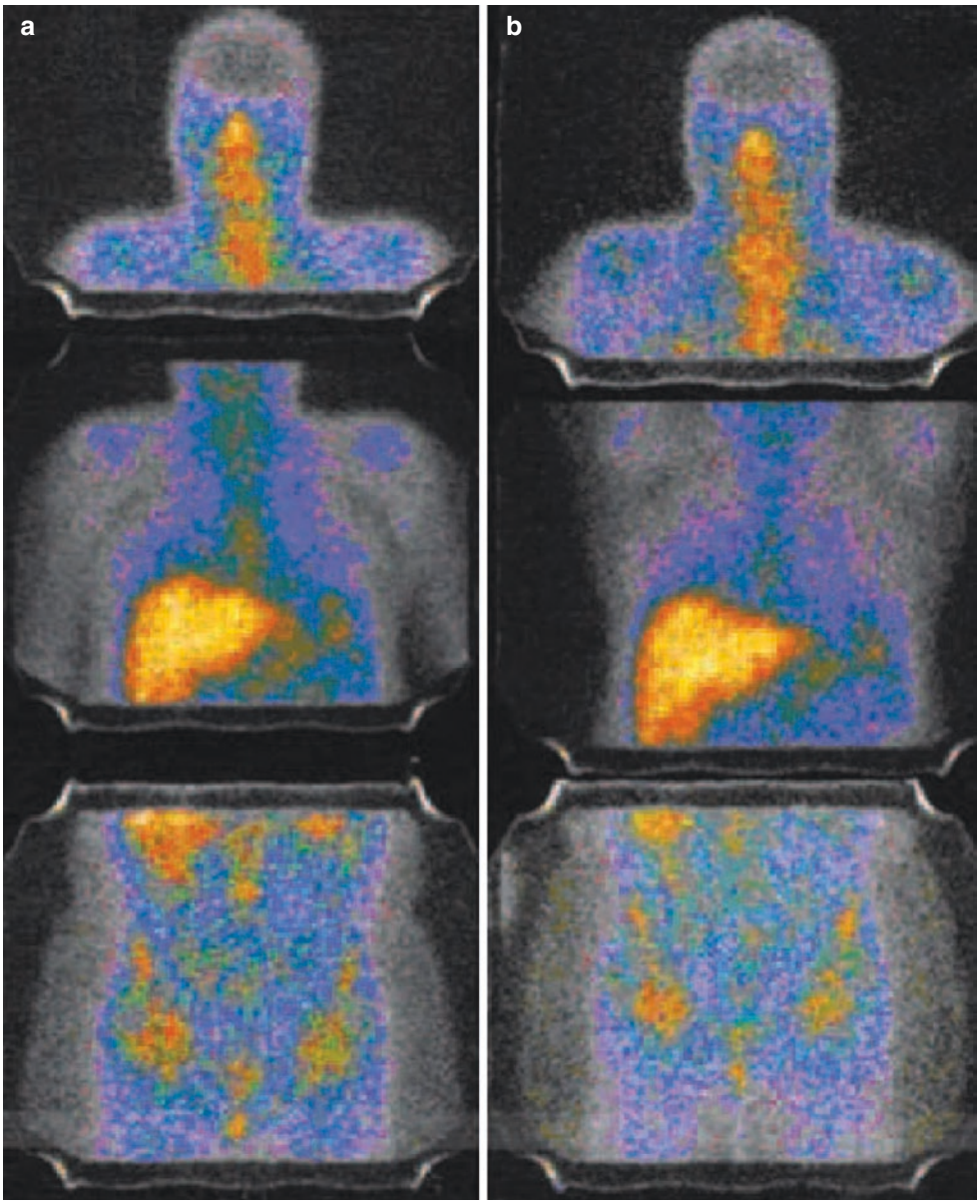

Fig. 1.3 Normal ^{67}Ga-citrate scintigraphy: anterior spot views of the head/neck (upper panels), chest (middle panels) and abdomen (lower panels) obtained 48 h (**a**) and 72 h (**b**) post-injection. Physiologic soft tissue visualization, with relatively intense tracer uptake in the liver (middle panels) and mild localization in pelvic bone and bone marrow (lower panels). Moderate radiopharmaceutical localization in the nasopharynx can also be seen (upper panels)

6. Recent chemotherapy and external beam radiation therapy [26].
7. Recent surgical wounds can induce increased radiopharmaceutical uptake, persisting up to 2 weeks after the event [29].
8. Uptake at cutaneous metal retention sutures, due to reaction at the site of insertion or other skin contact [29].
9. Desferoxamine therapy increases renal excretion of the tracer and enhances target-to-background ratios [30, 31].
10. Hilar, submandibular, and diffuse pulmonary localization in patients with lymphoma during therapy [20].
11. Radiation sialadenitis causes increased localization [32].
12. Possible uptake in a variety of tumors (i.e., lymphoma, lung cancer, mesothelioma, melanoma) [20, 33–37].
13. Physiologic liver uptake may be decreased in patients with AIDS or acute lymphocytic leukemia [26].
14. Diffusely increased pulmonary activity can occur in a variety of noninfectious disease as in cases of sarcoidosis, idiopathic pulmonary fibrosis, lymphoid interstitial pneumonitis, hypersensitivity pneumonitis, talc-induced granulomatosis, inhalational/occupational pulmonary diseases (asbestosis, berylliosis, coal worker pneumoconiosis, and silicosis), collagen vascular diseases (systemic lupus erythematosus and systemic sclerosis), eosinophilic pneumonia, multicentric reticulohistiocytosis, Wegener's granulomatosis, eosinophilic granuloma, drug toxicity (amiodarone, bleomycin, procarbazine, cyclophosphamide, nitrofurantoin, tocainide, busulfan), and reaction to iodinated contrast material (lipiodol) [38–62].

1.3 ^{99m}Tc-Diphosphonate (MDP/HDP) Scintigraphy

1.3.1 Normal Biodistribution of ^{99m}Tc-MDP/HDP

Excretion occurs primarily through the renal route, up to 70% of the injected activity being excreted within 6 h post-injection. Radiopharmaceutical uptake depends on local blood flow, osteoblastic activity, and extraction efficiency [6]. In a normal adult subject, the bone scan shows a higher concentration of activity in some parts of the skeleton, as in the spine (trabecular bone with large mineralizing bone surface), compared with the shafts of long bones (predominantly cortical bone) [63–68]. Renal and urinary bladder activities are normally present at the time of acquisition (about 3 h post-injection for a conventional bone scan) and minimal soft tissue activity is usually observed [6] (Fig. 1.4). This normal patten of distribution, however, is subject to considerable variation. In patients with significantly impaired renal function, the scans may be delayed to allow for better clearance of the extracellular fluid and vascular activity [67, 69].

1.3.2 Normal Variants in ^{99m}Tc-MDP/HDP Scintigraphy

1. Increased uptake at the confluence of sutures in the skull; this pattern can be more pronounced in patients with metabolic bone disease, such as renal osteodystrophy [65].
2. In elderly patients, increased uptake in the skull can be observed (especially in the frontal region and calvarium, due to hyperostosis frontalis interna) because of thickening of the frontal bones; such uptake can be more pronounced following chemotherapy in cancer patients, or in cases of metabolic bone disease [65].
3. Symmetrical or asymmetrical focal photopenia can be present in the parietal region, due to thinning of the parietal bone compared to the remaining portions of the skull [65].
4. Increased uptake at the manubriosternal junction [6].
5. A small photopenic defect (sternal foramina) surrounded by uniformly distributed radioactivity uptake can be observed in the inferior part of the sternum, due to the incomplete fusion of the cartilaginous bars in the distal sternum [65].
6. A vertical linear area of increased uptake can be seen distal to the sternum, due to benign tracer uptake in the xiphisternum [6].

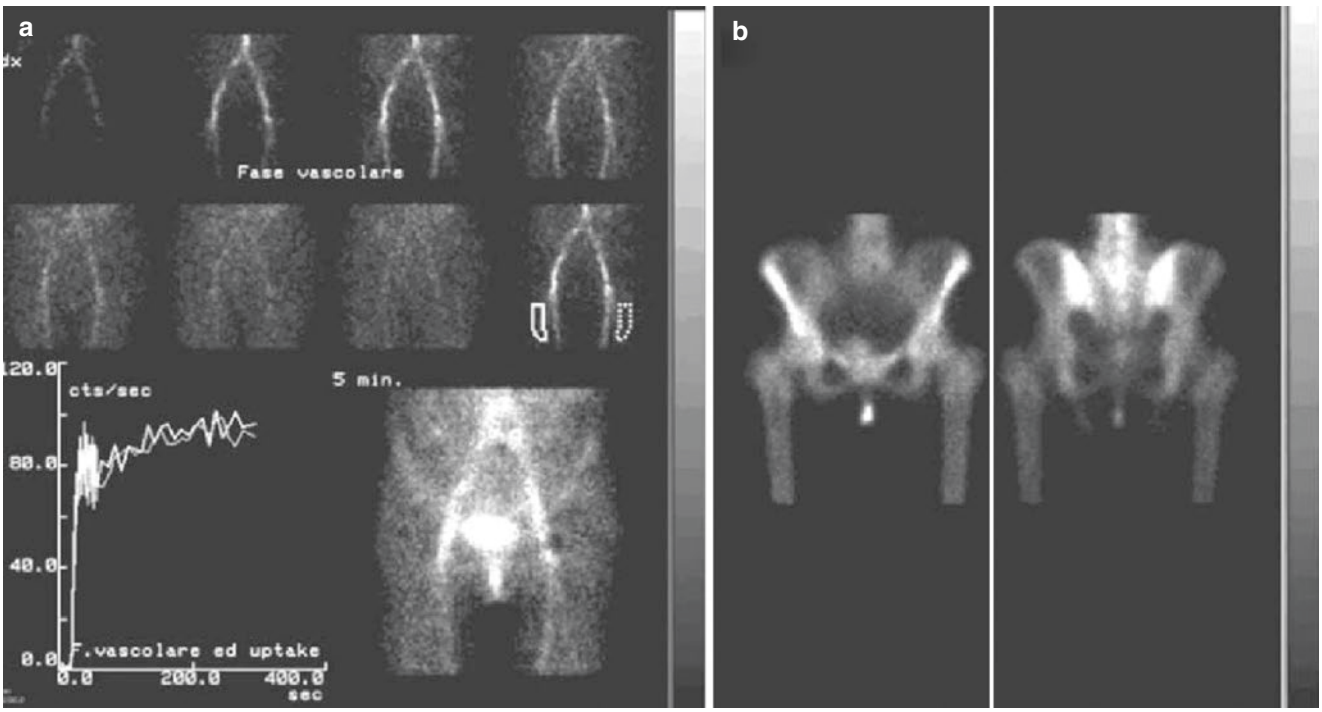

Fig. 1.4 ^{99m}Tc-MDP three-phase scintigraphy of the hip. (**a**) Arrival of the radiopharmaceutical in the region of interest; by drawing regions of interest (ROIs) on the suspected site of altered vascularization and on the corresponding contralateral, supposedly healthy site, it is possible to calculate time–activity curves. (**b**) Delayed scintigraphic acquisition (anterior and posterior images) obtained 3 h p.i., showing normal uptake of the pelvic bones

7. A focal area of increased uptake can be noted in the proximal/mid humeri at the site of insertion of skeletal muscles at the deltoid tuberosity [6].
8. Increased uptake in the pubic symphysis and possibly in the sacroiliac joints can be observed in women postpartum, as a consequence of increased stress reaction/pelvic diastases [65].
9. Diffuse breast uptake in women, especially if lactating [6].

1.3.3 Pitfalls in ^{99m}Tc-MDP/HDP Scintigraphy

1. Focally increased uptake in the mandible and/or maxillary bone is often due to underlying benign dental disorders [6].
2. Increased tracer uptake in the sinuses is frequently due to infection/inflammatory disease [6].
3. Hypertrophic pulmonary osteoarthropathy typically appears as symmetrically increased uptake of radiotracer in the cortices ("tram lines"), most often seen in the femora, tibiae, and wrists [6].
4. Decreased uptake in the presence of prosthesis (i.e., breast augmentation or orthopedic prosthesis) or metallic hardware (i.e., cardiac pacemaker), as well as at sites that have previously been included in an external beam radiation field [6].
5. Severe metabolic bone diseases may cause an abnormal radiopharmaceutical biodistribution (i.e., increased uptake at the confluence of head sutures, diffuse uptake in the calvarium) [65].
6. Symmetrical uptake in the acromioclavicular and/or sternoclavicular joint scan occur as consequence of degenerative disease [65].
7. Large vertical linear area of increased uptake in the sternum (sternal split) can be seen in patients who have undergone sternotomy [6].
8. A horizontal linear pattern of increased uptake in the vertebral body is typically observed in cases of vertebral fracture; however, it is difficult to distinguish fractures due to benign diseases, such as osteoporosis, from vertebral fractures due to a malignant condition [6].
9. Increased uptake in the patellae (hot patella sign), even if not be considered a real abnormal finding, can be seen in association with a wide variety of disorders, such as degenerative disease, Paget's disease, and osteomyelitis [65, 70].
10. In patients who have undergone recent surgery, such as knee or hip joint replacements, bone scintigraphy may result in false-positive findings [6].
11. Diffuse breast uptake in cases of gynecomastia induced by hormonal therapy in patients with prostate cancer. Focal breast uptake can be observed in other conditions, both benign and malignant [6].
12. Myocardial uptake can occur in case of myocardial necrosis/contusion, unstable angina, and ventricular aneurysm (focal pattern), or amyloidosis, hypercalemia, Adriamycin-induced cardiotoxicity, alcoholic cardiomyopathy, pericardial tumors, and pericarditis (diffuse pattern) [6].
13. Skeletal muscle uptake can be present in case of injury/trauma, renal failure, nontraumatic causes (i.e., alcoholic intoxication), scleroderma, polymyositis, carcinomatosis myopathy, muscular dystrophy, dermatomyositis, heterotopic bone formation/myositis ossificans (i.e., following direct trauma, complicated hip arthroplasty) [6].
14. Increased renal uptake can be observed after chemotherapy (vincristine, doxorubicin, cyclophosphamide) or in patients with nephrocalcinosis/hypercalcemia, iron overload, sickle cell disease, acute tubular necrosis (early stages), glomerulonephritis (diffuse pattern), and in the presence of obstructed collecting systems (focal pattern) [6].
15. Decreased renal uptake or non-visualization of the kidneys is generally observed as a consequence of nephrectomy, or in malignant/metabolic superscan. In cases of renal cyst, abscess, tumor, scarring as well as of partial nephrectomy, a focal area of reduced uptake can be observed [6].
16. Lung uptake can be observed in case of radiation pneumonitis, hyperparathyroidism, hypercalcemia, and, rarely, sarcoidosis [6].
17. Splenic uptake can be seen in case of Sickle cell disease, glucose-6-phosphtase deficiency, lymphoma, leukemia, and thalassemia [6].
18. Gastric uptake can be observed secondary to hypercalcemia with metastatic calcifications [6].
19. Bowel uptake can be observed in patients with surgical diversion, necrotizing enterocolitis, or ischemic bowel infarction [6].
20. Liver uptake can occur in the presence of amyloidosis and hepatic necrosis [6].
21. Soft tissue uptake can be observed in a variety of tumors (neuroblastoma, lung/liver tumors/metastases, breast tumors, sarcomas, malignant ascites/pleural effusion) [6].
22. Uptake in calcifications of the major arteries (i.e., femoral artery) [6].
23. Uptake in areas of cerebral infarct [6].

1.4 ^{99m}Tc-Sulfur Colloid and ^{99m}Tc-Albumin Nanocolloids

1.4.1 Normal Biodistribution of Radiocolloids

Following i.v. administration, the injected activity is rapidly cleared from the blood by the reticuloendothelial system (within approximately 2–4 h). About 55% of the

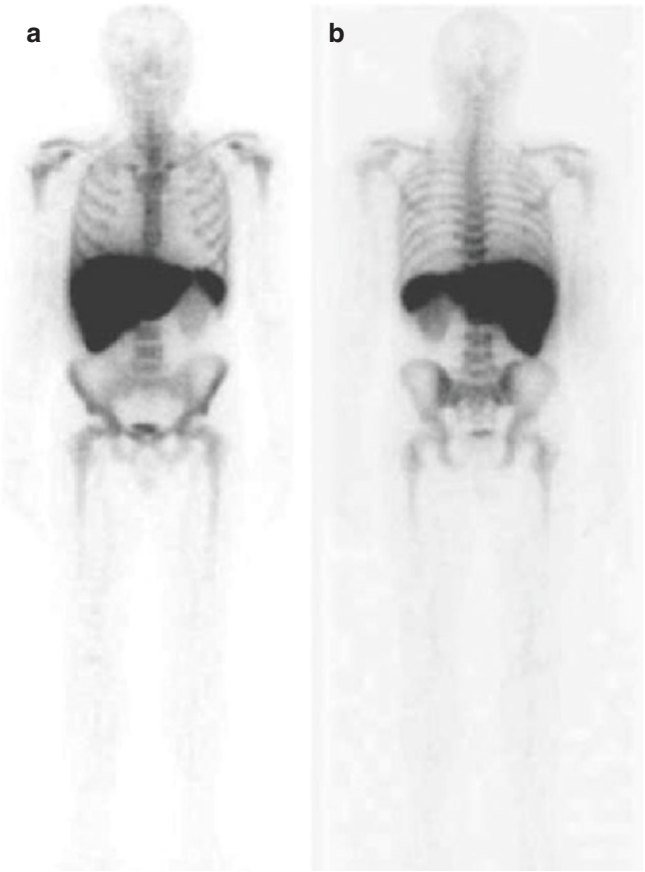

Fig. 1.5 Whole body scan following i.v. administration of 99mTc-albumin nanocolloids: anterior (**a**) and posterior (**b**) views show predominant uptake in the liver and spleen, with diffuse visualization of the hematopoietically active bone marrow

radiopharmaceutical is actively taken up by the reticuloendothelial system, to be degraded in the lysosomes of macrophages and excreted through the kidney within 24 h. An 80–90% of the injected particles is phagocytized by the Kupffer cells in the liver, 5–10% by macrophages in the spleen, and the remaining portion by macrophages in the bone marrow (see Fig. 1.5 for normal pattern of distribution as depicted in a whole body scan). However, uptake of the radiocolloid by the reticuloendothelial system is affected by both relative blood flow rates at the various sites and the functional capacity of the phagocytic cells, as well as by distribution of hematopoietically active marrow [21, 71].

1.4.2 Pitfalls in Radiocolloid Scintigraphy

1. Increased bone marrow uptake can be observed in case of aplastic anemia, myeloproliferative disease, and metastasis from solid tumors [72–74].

1.5 ^{99m}Tc-Besilesomab BW 250/183 (Scintimun®)

1.5.1 Normal Biodistribution of ^{99m}Tc-Besilesomab BW 250/183

About 10% of the injected activity is bound to neutrophils within 45 min post-administration, 20% of the radiopharmaceutical remaining free in the circulating blood. Up to 40% of the injected activity accumulates in the bone marrow [71, 75, 76] (see Fig. 1.6). Localization in the spleen, bowel, liver, bone marrow, thyroid, and kidney localizations is variable, occurring in up to 6%, to 4%, to 3%, and 2% of patients, respectively. Such normal distribution pattern is, however, subject to variation.

1.5.2 Pitfalls in ^{99m}Tc-Besilesomab BW 250/183 Scintigraphy

1. Physiological uptake in the bone marrow can mask small foci of infection located in the bone marrow space [71].
2. Spondylodiscitis and bone metastasis present as "cold" spots in the scan [75].
3. False-positive results can occur in case of myeloproliferative disease (i.e., multiple myeloma) [77].

1.6 ^{99m}Tc-Falonesomab (Leu-Tech®, NeutroSpec®)

1.6.1 Normal Biodistribution of ^{99m}Tc-Falonesomab

Following i.v. administration, activity is initially distributed in the circulating blood pool. The fraction bound to circulating neutrophils ranges between 11% and 51%, depending on neutrophil count. Bone marrow activity peaks shortly after administration (approximately 14% of injected activity at 2 h post-administration), with a longer washout time compared to background; the axial and appendicular bone marrow is well visualized. Spleen activity peaks at 5–12% of the injected amount 25–30 min post injection, declining to about half within 24 h. Similarly, rapid uptake is seen in the liver, with about 45–50% of the injected activity 35–65 min after administration, decreasing to 25–40% by 24 h. There is only minor retention of activity in the lungs [78]. Excretion occurs primarily through the renal route, radioactivity excreted in the urine being in the form of radiolabeled antibody fragments. Activity excreted through the gastrointestinal tract activity is variable [75, 79–82] (see Fig. 1.6).

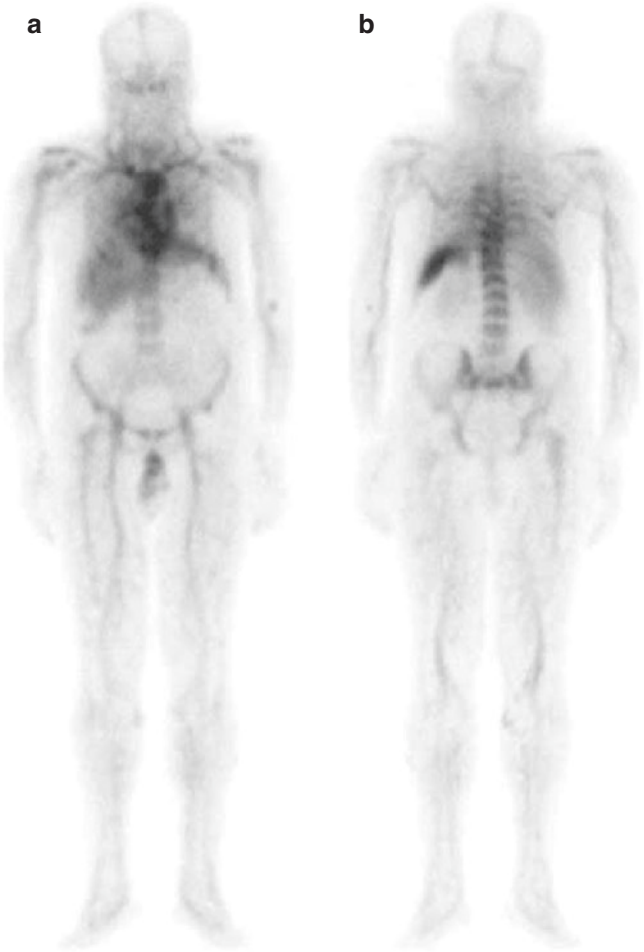

Fig. 1.6 Normal biodistribution of ^{99m}Tc-fanolesomab in the anterior and posterior views. Images obtained about 2 h after radiopharmaceutical administration (**a**) show activity within the cardiovascular system, genitourinary tract, liver, spleen, bone marrow, and soft tissues. By 24 h post injection of the radiolabeled antigranulocyte mAb, (**b**) blood pool activity has cleared and soft tissue activity has diminished, thus making bone marrow activity more prominent; diffuse colonic activity is also present. (Copyright permission from Love C et al. Imaging of infection and inflammation with ^{99m}Tc-fanolesomab. Q J Nucl Med Mol Imaging. 2006;50:113–20)

1.6.2 Pitfalls in ^{99m}Tc-Falonesomab Scintigraphy

1. Physiologic uptake in the bone marrow can mask small foci of infection located in the bone marrow space [71].

1.7 ^{99m}Tc-Sulesomab (LeukoScan®)

1.7.1 Normal Biodistribution of ^{99m}Tc-Sulesomab

About 25–34% of the injected activity circulates free in the blood 1 h after administration, declining to 17% at 4 h and 7% at 24 h. Activity bound to circulating granulocytes is more than 4% at 1 h post-injection. Bone marrow activity is about 43% at 1 h post-injection, the remaining activity being distributed in the liver, spleen, and kidneys (see Fig. 1.7). Excretion occurs virtually solely through the renal route, 41% of the injected activity being recovered in the urine over the first 24 h post-administration [81–84].

1.7.2 Pitfalls in ^{99m}Tc-Sulesomab Scintigraphy

1. Physiological uptake in the bone marrow can mask small foci of infection located in the bone marrow space [71].
2. Spondylodiscitis appears as a "cold" spot in the scan [75].
3. False-negative results can occur in the presence of orthopedic periprosthetic infection, chronic osteomyelitis (predominance of macrophages and lymphocytes over granulocytes) and abscess with impaired blood perfusion [85, 86].

1.8 ^{111}In-Oxine-Leukocyte Scintigraphy

1.8.1 Normal Distribution of ^{111}In-Oxine-Leukocytes

About 60% of the injected activity quickly localizes in the reticuloendothelial system of the liver, spleen, and bone marrow. There is only a transient migration of labeled cells in the lungs. The radiolabeled cells are cleared exponentially from the circulation, with a half-life between 5 and 10 h. Final distribution consists of about 20% of activity in the liver, 25% in the spleen, 30% in the bone marrow, and 25% in other organs. Images acquired up to 4 h post-injection may still show some pulmonary activity (Figs. 1.8 and 1.9). Clearance of activity from the liver and spleen is very slow. There is very low excretion of activity in both urine and feces, and no activity is normally observed in the bowel or bladder [87].

1.8.2 Normal Variants in ^{111}In-Oxine-Leukocyte Scintigraphy

1. Focal uptake can be seen in an accessory spleen [86].
2. Lymph node activity has been described in children—without however clinical significance [87–90].
3. Extramedullary hemopoiesis can result in lymph node activity [91].
4. Though usually solitary, multiple bilateral small round non-segmental lung foci of activity can occur, probably due to clumping of cells during the labeling process or during radiopharmaceutical injection; this occurrence may complicate interpretation of the images [85].

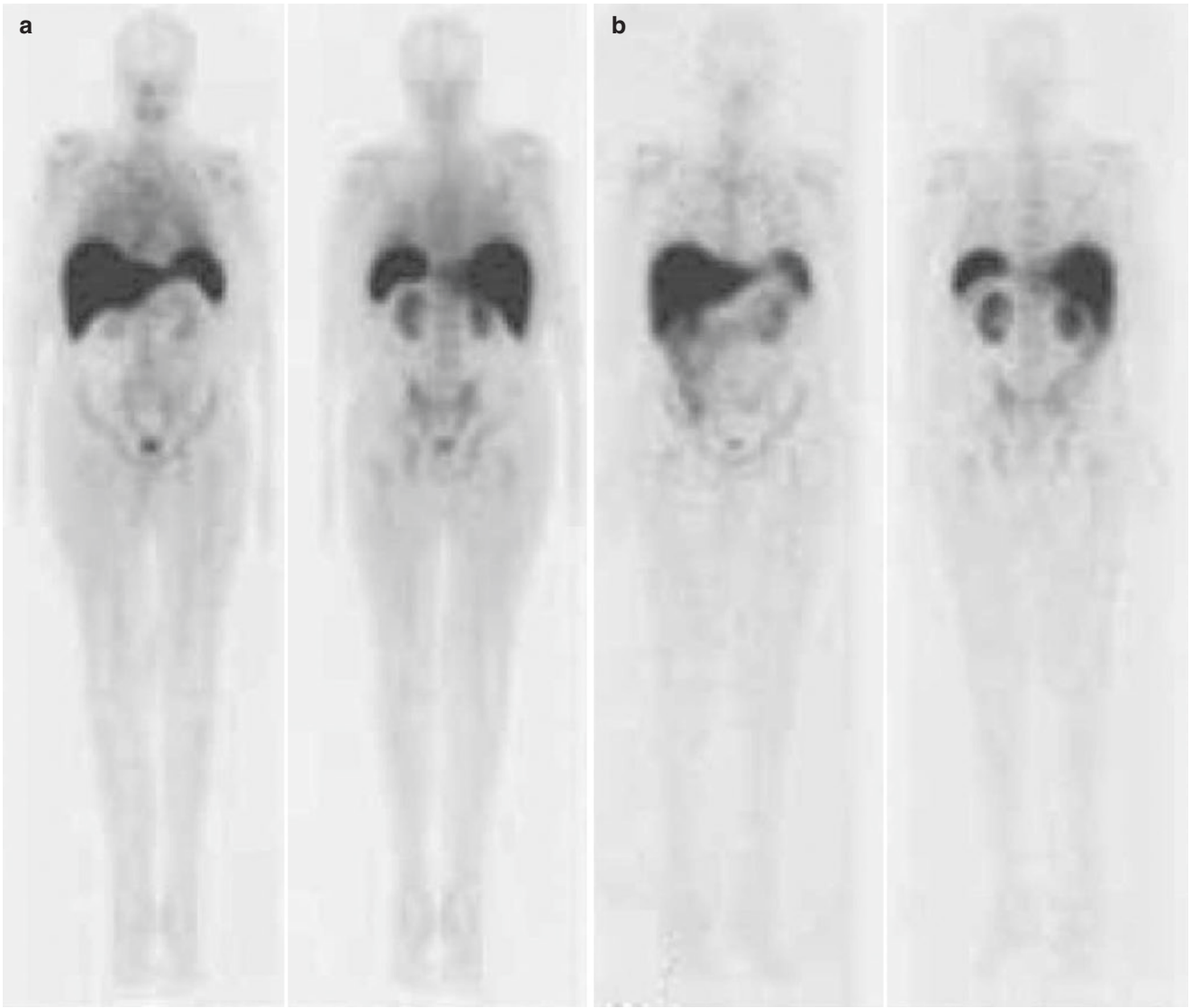

Fig. 1.7 ^{99m}Tc-Scintimun scintigraphy: anterior and posterior whole body images obtained 30 min (**a**) and about 3 h (**b**) post-injection, showing physiologic distribution of the radiopharmaceutical with uptake in the bone marrow, spleen, and liver; residual blood pool activity can also be seen

1.8.3 Pitfalls in ^{111}In-Oxine-Leukocyte Scintigraphy

1. In the presence of orthopedic hardware or prostheses, normal bone marrow is disrupted and displaced, making the interpretation of ^{111}In-oxine-leukocyte scintigraphy in these areas difficult [92].
2. Nonspecific bone/joint uptake can occur after bone marrow aspiration or at bone-graft donor sites and in the presence of traumatic/degenerative arthritis, gouty arthritis, acute fractures (less than 2 months), traumatic or neuropathic arthropathy, acute bone infarcts, or foreign body reaction. Although rarely, bone neoplasms (i.e., lymphoma with bone involvement) and metastasis, or active heterotopic bone formation can cause locally increased uptake [92–96].
3. Prolonged lung uptake can be observed when cells have been damaged during the labeling process.
4. Lung localization can be observed in cystic fibrosis and in patients with adult respiratory distress syndrome [85].
5. Focal uptake can be seen in cases of acute bleedings, hematomas, or recent myocardial/cerebral infarcts [21, 88].
6. Uptake can be observed in a variety of tumors (i.e., lymphoma, brain tumors) [92, 97].
7. Diffuse bowel uptake can occur in patients with non-infectious inflammatory bowel lesion(s) such as stomas, multiple enemas, gastrointestinal bleeding, or infarction [8].

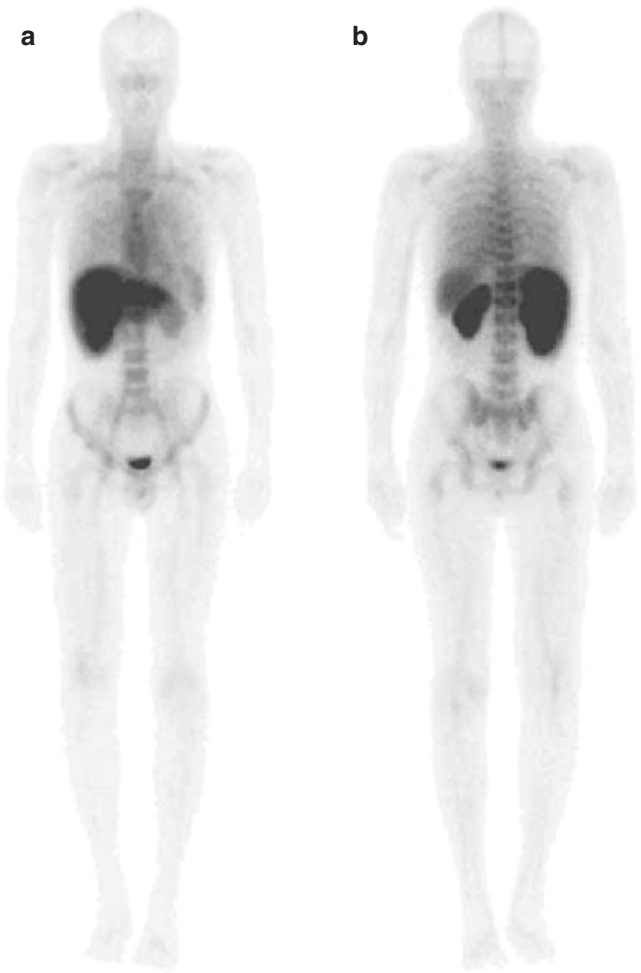

Fig. 1.8 ^{99m}Tc-Leukoscan whole body scan: the anterior (**a**) and posterior (**b**) views acquired 30 min p.i. show a physiologic pattern of distribution, with uptake in the bone marrow, liver, spleen, and kidneys

8. Chronic walled-off abscesses (more than 3 weeks since the onset), hepatic or splenic abscesses, lymphocytic mediated infection (i.e., granulomatous process, viral infection), low-grade or chronic osteomyelitis (especially in the central skeleton) are occasionally not visualized [98].
9. Abnormally decreased uptake can be seen in severely hypovascular/avascular sites (i.e., cysts, irradiated areas), implants (i.e., prostheses and cardiovascular implantable device), or spondylodiscitis (often appearing as focally decreased uptake compared with adjacent bone marrow) [21, 88, 99–101].
10. External beam radiation therapy induces intense, diffusely increased bone marrow activity at the site of treatment; after treatment, the irradiated sites appear as areas with decreased activity [99, 102].
11. Recent surgical wounds can appear as areas with increased uptake starting at approximately 72 h, with complete recovery in few days. When a surgical wound is not closed, or when it dehisces and is left to heal on its own by secondary intention, uptake persists as an area of intense accumulation—even in the absence of infection [21].
12. Noninfected vascular grafts and/or peritoneal shunts can show increased localization because of bleeding or noninfectious reparative process [103].

1.9 ^{99m}Tc-HMPAO-Leukocyte Scintigraphy

1.9.1 Normal Distribution of ^{99m}Tc-HMPAO-Leukocytes

The half-life of blood clearance of ^{99m}Tc-HMPAO-leukocytes is about 4 h. Bowel activity secondary to hepato-biliary secretion of ^{99m}Tc-complexes is usually not seen before 4 h; physiologic bowel activity is usually faint if seen at 4 h and is usually seen in the terminal ileum or right colon, increasing over time. The pulmonary uptake pattern of labeled leukocytes varies over time. Early images are characterized by diffuse pulmonary activity, which declines over time; by about 4 h post-injection, it becomes indistinguishable from background activity (Fig. 1.10). Renal and bladder activities are seen within 15–30 min post-injection in patients with normal renal function. Uniform physiologic gallbladder activity can be seen (in 4% of patients by 2–4 h and up to 10% of patients by 24 h). The spleen, liver, bone marrow, kidneys, bowel, bladder, and major blood vessels will normally be visualized [21, 71, 87].

1.9.2 Normal Variants in ^{99m}Tc-HMPAO-Leukocyte Scintigraphy

1. Bowel activity secondary to secretion of ^{99m}Tc-complexes can be detected in 20–30% of children as early as 1 h post-injection [102].

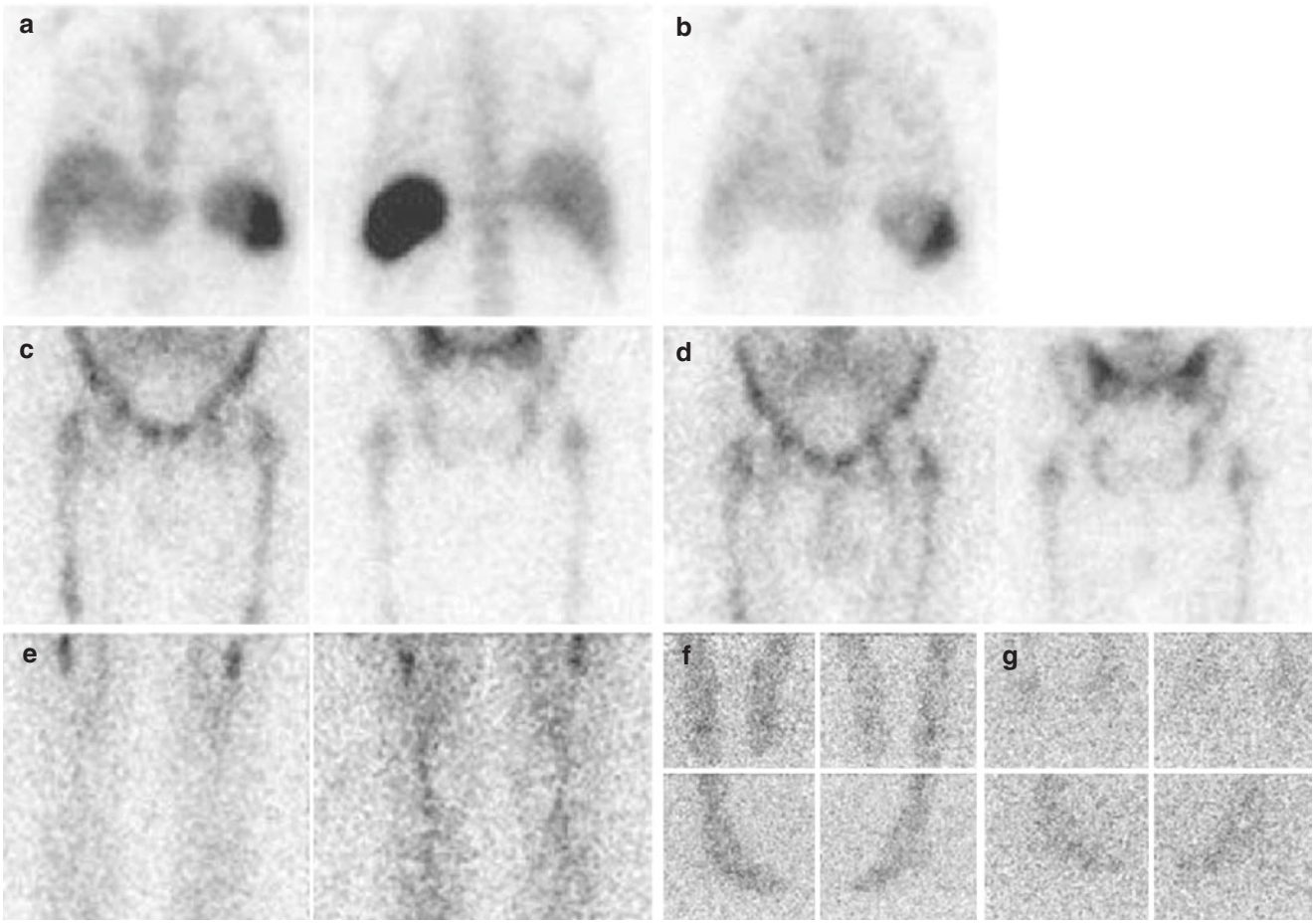

Fig. 1.9 ^{111}In-oxine-leukocyte scintigraphy. Planar spot views of the chest obtained 4 h (**a**) and 24 h (**b**) post injection. Early localization in the liver, spleen, and bone marrow (**a**), declining over time (**b**). Planar anterior and posterior spot views of the pelvis obtained 4 h (**c**) and 24 h (**d**) post injection show localization in the bone. Planar anterior and posterior views of the femora (**e**) obtained 24 h after administration show accumulation of the radiolabeled leukocytes in the bone marrow at the proximal portion of both femoral diaphyses. Planar spot views of the feet obtained 4 h (**f**) and 24 h (**g**) post injection obtained in anterior, posterior (upper panels) and lateral views (lower panels)

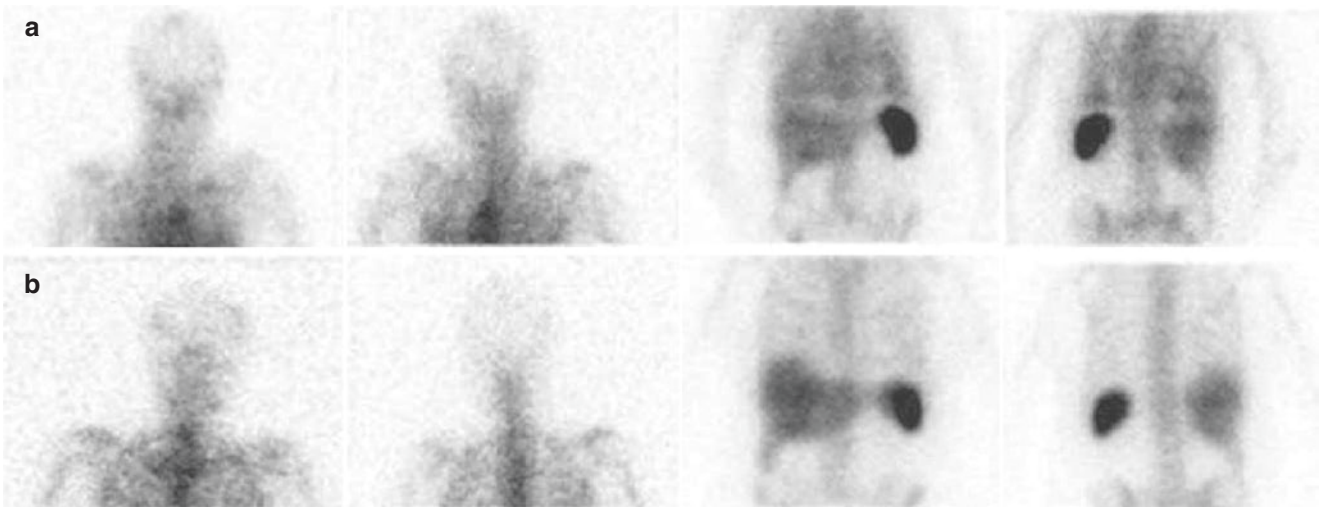

Fig. 1.10 ^{111}In-oxine-leukocyte scintigraphy: planar anterior and posterior spot views of the chest obtained 4 h (**a**) and 24 h (**b**) after radiolabeled leukocytes injection. Early images (**a**) show multiple bilateral small round non-segmental lung foci of activity due to cells clumping occurred during preparation/administration, a pattern that disappears in the later acquisitions (**b**). Activity in the liver, spleen, and bone marrow is also observed.
(Courtesy of Dr. Alberto Biggi, Cuneo)

2. Though usually solitary, multiple bilateral small round non-segmental lung foci of activity can occur, probably due to clumping of cells during the labeling process or during injection; this occurrence complicates interpretation of the scan [94].
3. Focal uptake can be seen in the presence of accessory spleen(s).

1.9.3 Pitfalls in ^{99m}Tc-HMPAO-Leukocyte Scintigraphy

1. Bone marrow expansion or hyperplasia can alter the normal scintigraphic patterns of bone marrow visualization [21, 100].
2. Lung activity can be present at 3 h post administration in case of pulmonary edema, diffuse inflammatory lung disease as pulmonary drug toxicity (bleomycin, methotrexate, and paclitaxel), atelectasis, radiation pneumonitis, heart or renal failure, sepsis, or adult respiratory distress syndrome, or due to cell damage during labeling [20, 87, 104–108].
3. Focal uptake can be seen in case of neoplasms (i.e., lymphoma, brain tumors) or hematomas [94, 109].
4. Spondylodiscitis may lead to either a spot of increased activity or more often a "cold" spot as compared with normal bone marrow localization [21, 110].
5. A "cold" spot in the spine may occur in the presence of compression fracture, neoplasm, post-irradiation changes, or postsurgical or anatomic deformities [94].
6. Bowel activity (prior to 4 h) can occur from intraluminal transit of labeled cells secondary to active gastrointestinal bleeding [21].
7. Normal renal activity can make it difficult to detect pyelonephritis and/or a renal abscess [104].
8. Chronic walled-off abscesses or low-grade infections, particularly in bone, have reduced the accumulation of ^{99m}Tc-HMPAO-granulocytes and are more likely not to be visualized in the scan [20, 111].
9. Non-infected vascular grafts and/or peritoneal shunts can show increased localization because of bleeding or non-infected reparative process [103].
10. Recent surgical wounds can induce increased uptake by approximately 72 h, with complete resolution in few days. When a surgical wound is not closed, or when it dehisces and is left to heal on its own by secondary intention, uptake persists and appears as areas of intense activity even in the absence of infection [21].

1.10 [^{18}F]FDG PET/CT (and PET/MR)

1.10.1 Normal Biodistribution of [^{18}F]FDG

[^{18}F]FDG uptake is physiologically most intense in the brain because of predominant glycolytic metabolism in neurons; uptake in the myocardium is variable, since the primary energy source for myocardiocytes is fatty acids. Since [^{18}F]FDG is excreted by the kidney into the urine, intense [^{18}F]FDG activity is normally observed in the intrarenal collecting systems, ureters, and bladder. Even 1 h after administration, the urinary excretion of [^{18}F]FDG continues in well-hydrated patients. Less intense and variable physiologic activity is present in the liver, spleen, bone marrow, and renal cortex. At 1 h post-injection, blood pool activity results in a moderate activity in the mediastinum against a low background lung activity (Fig. 1.11). Uptake in skeletal muscles is generally low if the patient has been allowed sufficient rest after physical activity before tracer injection. The larynx and vocal cords usually show either no uptake or mild symmetric uptake, which may have an inverted U shape [17, 111, 112].

1.10.2 Normal Variants in [^{18}F]FDG PET/CT

1. Gastrointestinal activity may have variable intensity and pattern related to multiple factors including muscular peristaltic activity, presence of lymphoid tissue (particularly in the cecum), high concentration of white blood cells in the bowel wall, swallowed secretions, intraluminal concentration of [^{18}F]FDG, colonic microbial uptake, drug interference (i.e., metformin) [113].

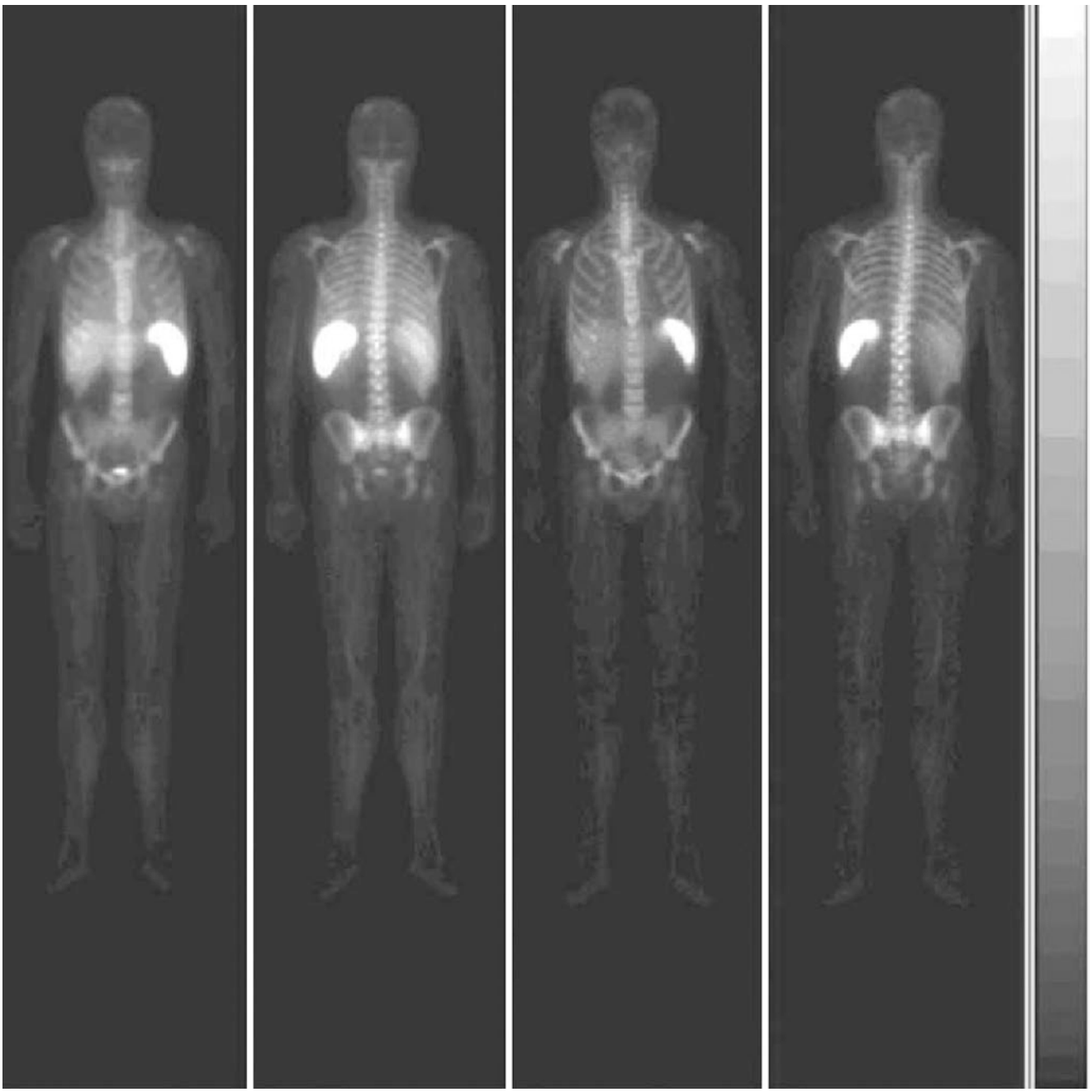

Fig. 1.11 ^{99m}Tc-HMPAO-leukocyte scintigraphy: anterior and posterior whole body images acquired 30 min p.i., showing physiologic uptake of labeled leukocytes in the spleen, liver, and bone marrow

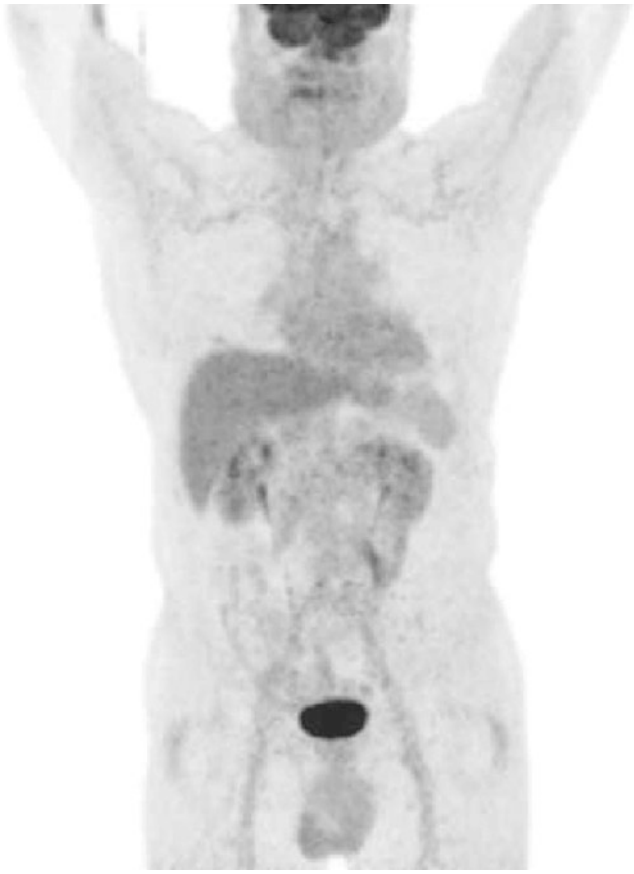

Fig. 1.12 PET/CT MIP image obtained 60 min after [^{18}F]FDG injection shows the physiologic pattern of biodistribution of this metabolic tracer

2. Intense uptake can be observed in the brown adipose tissue, commonly present symmetrically in the midaxillary line, posterior mediastinum, supra-clavicular, peri-hepatic, and para-spinal regions [114, 115] (Fig. 1.12).
3. Prominent activity in the laryngeal structures can occur in case of excessive talking while waiting after tracer injection, before the scan [112] (Fig. 1.12).
4. Cardiac activity is variable, ranging from no discernible activity above background blood pool activity to intense activity throughout the left ventricular myocardium, even in the fasting state [116]. Increased activity can present with a diffuse pattern (with/without heterogeneity), focally (i.e., papillary muscles), or regionally [116] (Fig. 1.13).
5. Physiologic thymic uptake can be observed in childhood, until puberty [117].
6. Mild to moderate uptake is usually seen in the adenoids, in the tonsils, and at the base of the tongue in children, due to the physiologic activity of lymphatic tissue in the Waldeyer ring [116]; this occurrence peaks around 6–8 years of age, declining then with increasing age.
7. Patients in the pediatric age range may have physiologic linear uptake in ephyses and apophyses, due to skeletal growth [110].
8. In children, uptake in the salivary glands is variable, but typically mild to moderate [115].
9. Endometrial uptake may increase during the ovulatory and menstrual phases in premenopausal women [17].
10. Moderate and diffuse uptake can be seen in the breasts, higher in adolescent girls with dense breasts or in lactating breasts (Fig. 1.14). Also the nipples normally demonstrate some activity uptake, better identified in the non-attenuation-corrected images [118].
11. Testicular uptake is usually symmetrical and diffuse, and it may decrease with age [119] (Fig. 1.15).
12. Increased uptake in skeletal muscles (generally symmetric) can occur due to excessive muscle activity during the uptake phase, or within a few days preceding the PET scan [112] (Fig. 1.16).

1.10.3 Pitfalls in [^{18}F]FDG PET/CT

1. Hyperinsulinemia may result in a "muscle scan" [120] (Fig. 1.17).
2. A well-defined focus of uptake in the lung on [^{18}F]FDG-PET without a detectable corresponding abnormality on the integrated CT (either above or below the diaphragm) can be observed as a consequence of microemboli secondary to paravenous injection. Since the blood clots are admixed with injected radiotracer, they may be very intense [120].
3. Increased bowel uptake can be seen in chronic inflammatory conditions, such as enterocolitis and inflammatory bowel disease [17].
4. Markedly increased uptake along the esophagus can occur in patients with esophagitis or after radiation therapy, or in patients with hiatal hernia and Barrett esophagus (in the distal esophagus) [112].
5. Focal pooling can be observed in renal calyces/pelvis, dilated/redundant ureters and bladder diverticula [17] (Fig. 1.18).
6. Diffuse myocardial uptake can occur in the presence of several myocardial diseases, including systemic and pulmonary hypertension, and valvular heart disease. Also myocarditis, both infective and radiation-induced, manifests as diffuse myocardial uptake. Increased activity localized in the atria is associated with atrial fibrillation. Myocardial and pericardial tumors and metastasis appear as focal [^{18}F]FDG uptake. The physiologic patterns of biodistribution of [^{18}F]FDG can mimic coronary ischemia. Left bundle-branch block is associated with a pattern of decreased [^{18}F]FDG septal activity. Radiation-induced pericarditis may result in a pattern of diffuse

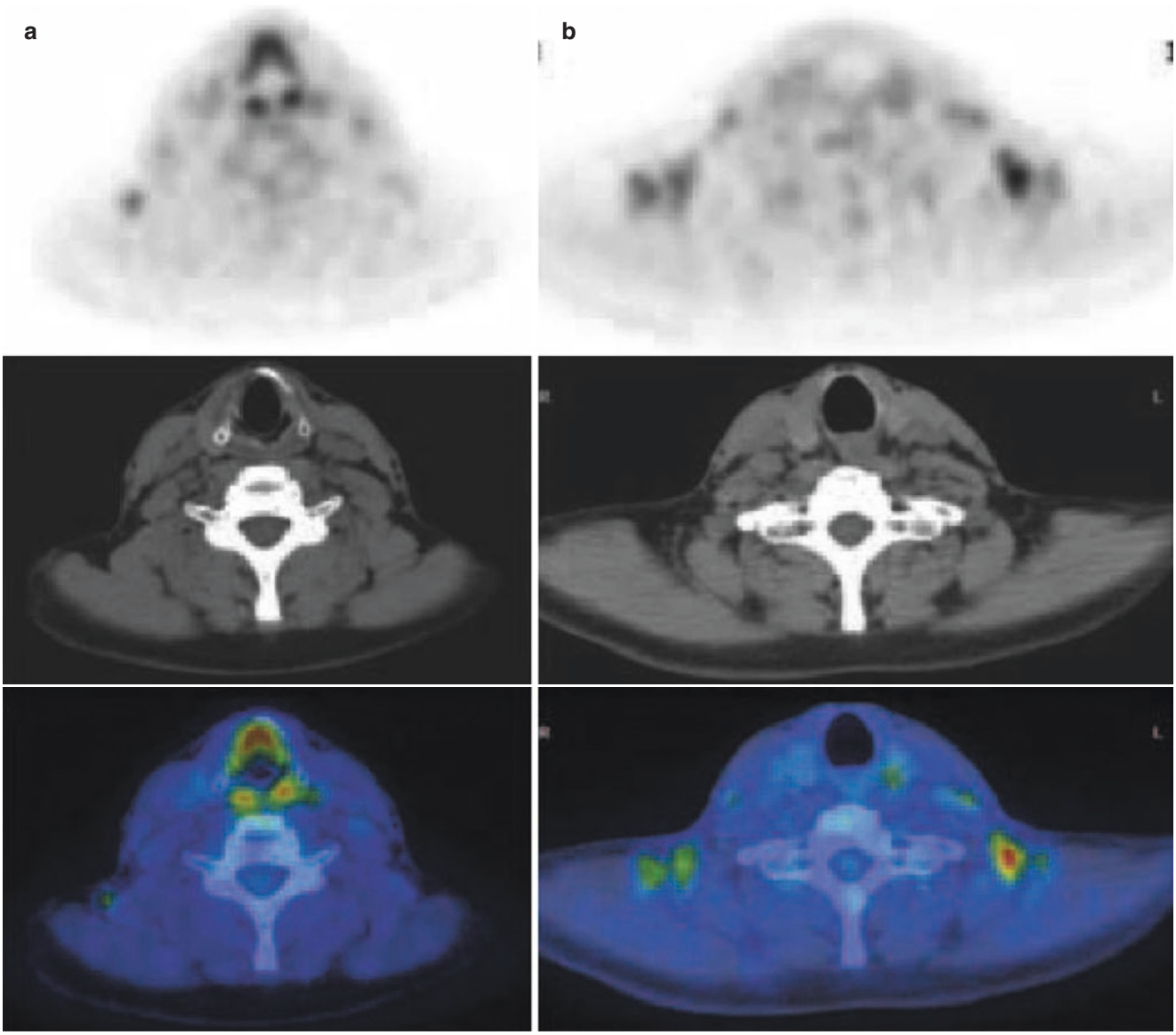

Fig. 1.13 [^{18}F]FDG-PET/CT images (PET component in upper panels, CT component in middle panels, and fused PET/CT images in lower panels) showing two normal variants of [^{18}F]FDG uptake in the same patient. (**a**) [^{18}F]FDG uptake at the epiglottis and arytenoid muscles, due to excessive talking during waiting time between tracer injection and scan acquisition. (**b**) Increased uptake in the thermogenic brown fat of the sovraclavear regions (more prominent on the left side in this particular case)

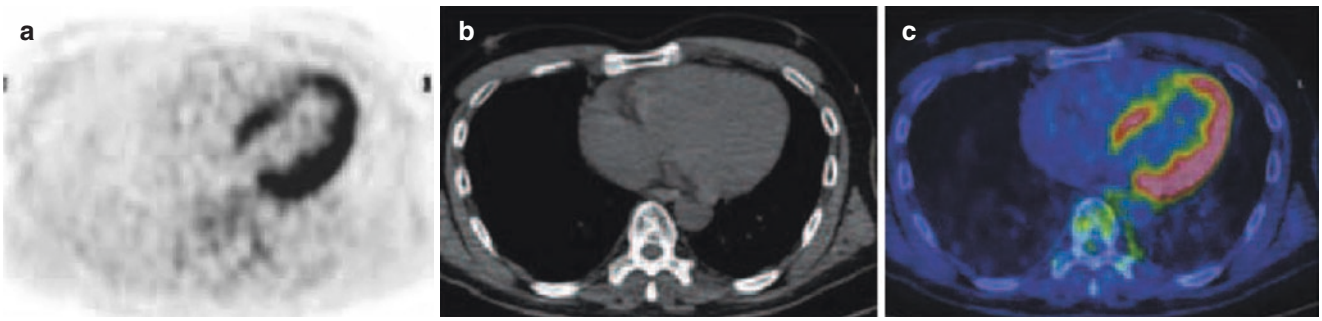

Fig. 1.14 Transaxial [^{18}F]FDG PET/CT images [PET component in left panel (**a**), CT component in middle panel (**b**), fused PET/CT image in right panel (**c**)], showing intense myocardial [^{18}F]FDG uptake, but with an area of reduced uptake in the septum in a patient with left bundle-branch block